# 9-Ethyladenine: Mechanochemical Synthesis, Characterization and DFT Calculations of Novel Cocrystals and Salts

Contribution from:

Yannick Roselló[†], Mónica Benito[‡], Núria Bagués[‡], Núria Martínez[‡], Alba Moradell[‡], Ignasi Mata[‡], Judit Galcerà[‡], Miquel Barceló-Oliver[†], Antonio Frontera[†*], Elies Molins[‡*]

[†]Departament de Química, Universitat de les Illes Balears, Ctra. Valldemosa km 7.5, E-07122 Palma de Mallorca, Spain

[‡]Institut de Ciència de Materials de Barcelona (ICMAB-CSIC), c/ Til·lers, 1, Campus UAB, 08193 Bellaterra, Spain

KEYWORDS: 9-ethyladenine, crystal engineering, cocrystal, nucleobases, mechanochemistry, grinding, physical characterization, DFT, QTAIM.

## ABSTRACT

Liquid-assisted grinding and solvent crystallizations have been undertaken to prepare salts and cocrystals of the modified nucleobase 9-ethyladenine with several carboxylic acids. The new solid forms have been characterized by X-ray powder and single crystal diffraction, attenuated total reflectance Fourier transformed infrared spectroscopy and thermal methods. From single crystal structures we have observed that the length of the alkylic chain in the carboxylic acid prevents from a canonical self-assembly for the longest coformer. Moreover, density functional theory (DFT) calculations combined with

the quantum theory of "Atoms-in-Molecules" QTAIM have been performed to analyze the different binding modes of adenine and the energetic features of the complexes. In particular, the interaction energies of several adenine dimers and trimers, and also the hydrogen-bonds with carboxylic acids interacting with Watson-Crick and Hoogsten faces of adenine, have been computed and compared.

## INTRODUCTION

In the last century, mechanochemistry has emerged as an extraordinary, versatile, effective and green technique for the preparation of new and different types of materials including not only pharmaceutical solids, such as salts and cocrystals,[1,2] but also for batteries,[3] catalysts,[4,5] metal-organic frameworks (MOFs),[6] organic synthesis[7] and others.[8] In this sense, through a mechanochemical process, forces such as compression, shear or friction can provoke chemical transformations resulting an attractive alternative to synthesis in solution and in some cases leading to different products.[9]

At lab scale mechanochemical synthesis can be performed simply by hand grinding with a pestle and a mortar or by ball milling adding the starting reactants and one or several balls in a milling jar, as done in a ball mill. Alternatively, when higher amounts of product are required, the preferred option is the use of planetary mills. The results may be modulated through several parameters: the type of material for the balls and the grinding jars, the frequency, the duration time or even the amount ratio among reactants and balls. Finally, the addition of a few drops of solvent, known as solvent-drop grinding, can ameliorate drastically the process specially for cocrystal screenings.

On the other hand, cocrystallization has desmonstrated to be an effective way to improve the physicochemical properties of drugs without altering their intrinsic pharmacological behavior. At early in the pharma industry, some strategies for solving drawbacks related

to solubility, intrinsic dissolutions, stability, hygroscopicity included salt screenings or even coamorphization.[10-11] But in the last decades, cocrystals have emerged as a valuable alternative just by tailoring the coformers used.[12]

Recognition among DNA nucleobases and also with other small molecules started in the middle fifties from the last century with the work of Hoogsteen[13] and were later followed by others.[14-20] During all this time, great efforts from the crystal engineering point of view have been done to fully understand protein-nucleic acid recognition.

However, the use of solid state grinding to prepare cocrystals containing nucleobases was not reported until the nineties by Etter *et al*.[21] After that, cocrystals and salts of different nucleobases or analogs have been reported with the goal of understanding which interactions are prevalent.[22-25]

9-ethyladenine, or 6-amino-9-ethylpurine, is a modified purine base which its single crystal structure was early described.[14,26] Its ability to form hydrogen-bonded complexes through its Watson-Crick or Hoogsteen faces and its reproducing base pair recognition, as in DNA with other natural or modified nucleobases, has been explored in the past.[14-18, 26-27]

In this work we report the use of this modified nucleobase, 9-ethyladenine, as building block molecule for hydrogen bond recognition with several dicarboxylic acids using liquid assisted grinding (LAG) technique, as the main screening technique. We have explored its ability to form salts and/or cocrystals, the predominant synthons in the solid state and how they influence the crystal packing. It is important to highlight that the binding modes reported herein for the nucleobase and the carboxylic acids can be used as models for possible recognition of DNA/RNA with proteins *via* the side chains of Aspartic and Glutamic amino-acids.[28]

The molecular structure of 9-ethyladenine (9ETADE) and the coformers used are displayed in Scheme 1. These are malonic (MAL), succinic (SUC), glutaric (GLU), adipic (ADI) and fumaric (FUM) acids. All of them are included in the list of pharmaceutically acceptable acids based on the *Handbook of Pharmaceutical Salts*[29] and show different p$K_a$ values. The widely p$K_a$ rule will be used to foresee their ability for the preparation of salts or cocrystals.

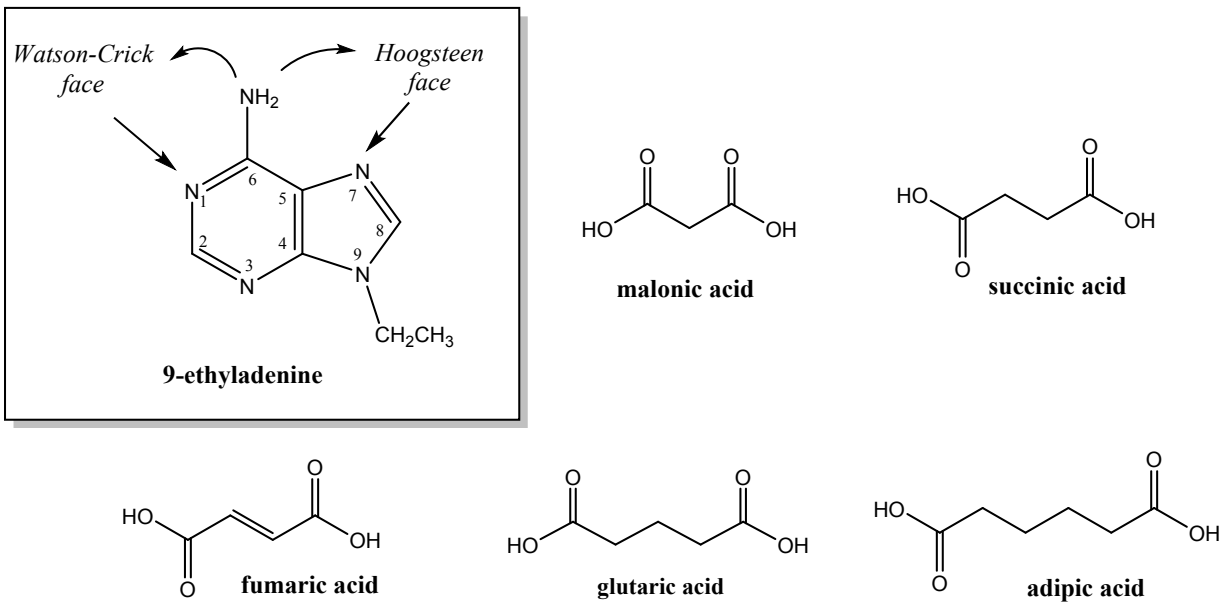


**Scheme 1. Molecular structures of 9-ethyladenine and the coformers described in this study.**

## EXPERIMENTAL METHODS

All reagents were purchased from Sigma-Aldrich Co., Panreac and VWR International. Analytical grade solvents were used for the liquid-assisted grinding or crystallization experiments. All materials were used without any further purification.

*Synthesis of 9-ethyladenine*. The modified adenine was obtained by treatment of adenine with bromoethane using sodium hydride as base following the previous synthesis described for the preparation of 9,9-trimethylenbisadenine.[30]

**Screening by liquid assisted grinding.** Mechanochemical synthesis of cocrystals and salts were performed using a Retsch ball mill MM400 in 10 mL agate grinding jars with two 5 mm agate balls. 1:1 and 2:1 stoichiometric ratio of 9-ethyladenine and the selected coformer were ground for 30 min at 30 Hz with two drops of water (for compounds **1**-**7**) or methanol (for **2**-**3** and **6**). See experimental details in the Supplementary Information.

**Single crystal preparation by evaporative crystallizations.** Slow evaporations were carried out to obtain single crystals of the new solid forms. See experimental details in Supplementary Information.

**Powder X-ray Diffraction (PXRD).** PXRD data were collected using a Siemens D5000 powder X-ray diffractometer with Cu-Kα radiation (λ = 1.54056 Å), with 35 kV voltage and 45 mA current applied. An amount of powder was gently pressed on a glass slide to afford a flat surface and then analyzed. The samples were θ-2θ scanned from 2 to 50° using a step size of 0.02° and a scan rate of 1 step/s.

**Single Crystal X-ray Diffraction (SC-XRD).** Suitable crystals of **2**, **4** and **5** were selected for the X-ray single crystal diffraction experiments, covered with oil (Infineum V8512, formerly known as Paratone N) and mounted at the tip of a nylon CryoLoop on an Oxford Diffraction Xcalibur system with a Ruby detector using graphite monochromated MoKα radiation (λ = 0.7107 Å). Crystallographic data were collected at 183(2) K. The program suite CRYSALISPro was used for data collection, Lorentz-polarization and semi-empirical absorption corrections and data reduction.[31]

When observed in the microscope, crystals of **7** seem composed of thin superposed plates. One specimen considered suited for X-ray single crystal diffraction was covered with oil (Infineum V8512, formerly known as Paratone N) and mounted at the tip of a nylon CryoLoop on a BRUKER-NONIUS X8 APEX-II KAPPA CCD diffractometer using graphite monochromated MoKα radiation (λ = 0.7107 Å). Crystallographic data were collected at 300(2) K. In the experiment, it was observed that diffraction peaks were elongated in one direction, probably because of high mosaicity in the direction of the stacking of the plates. In spite of this inconvenience, diffraction peaks could be integrated and merged. Data were corrected for Lorentz and polarisation effects and for absorption by SADABS.[32]

Suitable crystals of **1**, **3** and **6** were selected for X-ray single crystal diffraction experiments and mounted at the tip of a glass fibre on an Enraf-Nonius CAD4 diffractometer producing graphite monochromated MoKα radiation (λ = 0.7107 Å). After the random search of 25 reflections, the indexation procedure gave rise to the cell parameters. Intensity data were collected in the ω-2θ scan mode at 293(2) K. Data were corrected for Lorentz and polarization effects. The absorption correction was performed following Gaussian quadrature method (**6**)[33] or DIFABS (**1** and **3**)[34].

The structural resolution procedure was made using the WinGX package.[35] Solving for structure factor phases was performed by SHELXS-2013[36] (**1**, **3**, **6**), SHELXS-97[36] (**4**), SIR97[37] (**2** and **5**) and SHELXT-2014[38] (**7**). For the full matrix refinement SHELXL2018/3[38] (**1**, **3**, **6**) or SHELXL-2017/1[38-39] (**2**, **4**, **5** and **7**) were used. The structures were checked for higher symmetry with help of the program PLATON.[40] The software CRYSALISPro was used for treating **4** as a twinned crystal, generating separated reflection sets for each one of the twins. The twin is formed by two components connected by a 2-fold axis perpendicular to (100) with fractional contributions 0.36:0.64. Non-H atoms were refined anisotropically. For **3**, H-atoms were introduced in calculated

positions and refined riding on their parent atoms. For **1**, H-atoms were introduced in calculated positions and refined riding on their parent atoms, except for H-atoms from the water molecule, which were located in the Fourier map and refined isotropically with Uiso(H) = 1.5Ueq(O). For **2**, H-atoms bound to carbons were introduced in calculated positions and refined riding on their parent atoms, and H-atoms bound to nitrogen and oxygen atoms (H6A and H6B and protonation sites (H1 and H30)) were located in the Fourier map and refined isotropically with Uiso(H) = 1.5Ueq(N,O). For **4**, **5** and **7**, H-atoms were introduced in calculated positions and refined riding on their parent atoms except for the protonation sites, which were located in the Fourier map and refined isotropically with Uiso(H) = 1.5Ueq(N,O). For **6**, H-atoms were refined isotropically with fixed Uiso(H) = 1.2Ueq(C) and 1.5Ueq(N,O). In Table 1 general and crystallographic data for the salts and cocrystals described in this work are summarized. Hydrogen-bond data for all the solved structures can be found in Supplementary Information (Table S1). In the case of **7**, the thermal ellipsois are slightly elongated in the direction (101), which can be attributed to the high mosaicity of the crystal in this direction. As can be seen in the Results and Discussion section, the crystal packing of **7** consists on layers parallel to (101) and weakly bounded between them, which can be the origin of this high mosaicity. This is surely the cause of the resulting high R factors in **7** (Table 1). As these are the best crystals we could obtain from different essays, the conformation of the layers of **7** will be discussed in the next section as they are properly described by the model.

**Table 1**. **General and crystallographic data for prepared salts and cocrystals.**

| **Compound** | **(1)** | **(2)** | **(3)** | **(4)** | **(5)** | **(6)** | **(7)** |
|---|---|---|---|---|---|---|---|
| Formula | C10 H15 N5 O5 | C11 H15 N5 O4 | C9 H12 N5 O2 | C12 H17 N5 O4 | C22 H30 N10 O10 | C18 H22 N10 O4 | C13 H19 N5 O4 |
| mol wt | 285.26 | 281.28 | 222.24 | 295.30 | 594.56 | 442.43 | 309.33 |
| T (K) | 293(2) | 183(2) | 293(2) | 183(2) | 183(2) | 293(2) | 299(2) |
| λ (Å) | 0.71073 | 0.71073 | 0.71073 | 0.71073 | 0.71073 | 0.71073 | 0.71073 |
| Crystal system | Triclinic | Triclinic | Monoclinic | Monoclinic | Monoclinic | Monoclinic | Monoclinic |
| Space group | P -1 | P -1 | P 21/n | P 21/c | C 2/m | P 21/n | P21/c |
| a (Å) | 6.819(8) | 5.1697(2) | 9.891(4) | 10.6126(17) | 19.756(3) | 15.575(1) | 11.943(2) |
| b (Å) | 8.167(7) | 10.9731(9) | 8.478(3) | 19.783(2) | 6.5260(4) | 8.707(3) | 20.440(4) |

| | | | | | | | |
|---|---|---|---|---|---|---|---|
| c (Å) | 13.105(5) | 11.3150(4) | 12.803(5) | 6.8213(19) | 13.680(6) | 15.741(2) | 13.308(2) |
| α (°) | 88.16(5) | 96.1307(4) | 90 | 90 | 90 | 90 | 90 |
| β (°) | 75.49(6) | 91.253(3) | 97.66(4) | 106.07(2) | 131.372(11) | 97.08(1) | 108.715(3) |
| γ (°) | 71.68(10) | 98.379(5) | 90 | 90 | 90 | 90 | 90 |
| V (Å$^3$) | 669.9(11) | 630.94(6) | 1064.0(4) | 1376.2(5) | 1323.5(7) | 2118.4(8) | 3077.0(10) |
| Z | 2 | 2 | 4 | 4 | 2 | 4 | 8 |
| D (Mg/m$^3$) | 1.325 | 1.481 | 1.387 | 1.425 | 1.492 | 1.387 | 1.335 |
| μ (mm$^{-1}$) | 0.105 | 0.115 | 0.103 | 0.109 | 0.120 | 0.137 | 0.101 |
| F(000) | 300 | 296 | 468 | 624 | 624 | 1168 | 1312 |
| Reflns/unique | 2727/2615 | 4596/2486 | 3090/2085 | 2713/2713 | 5262/1428 | 4305/4152 | 31689/5830 |
| R(int) | 0.0419 | 0.0250 | 0.0334 | 0.0496 | 0.0311 | 0.0283 | 0.0501 |
| Data/restraints/params | 2615 / 3 / 191 | 2486 / 0 / 194 | 2085 / 0 / 147 | 2713 / 0 / 198 | 1428 / 5 / 135 | 4152 / 22 / 340 | 5830 / 4 / 411 |
| GOF on F$^2$ | 1.006 | 0.856 | 0.978 | 0.862 | 1.101 | 0.817 | 1.621 |
| $R_1$, $wR_2$ [I>2σ(I)] | 0.0668, 0.1818 | 0.0400, 0.0728 | 0.0568, 0.1272 | 0.0506, 0.0916 | 0.0710, 0.2284 | 0.0632, 0.1273 | 0.1508,0.3728 |
| $R_1$, $wR_2$ (all data) | 0.1082, 0.2025 | 0.0743, 0.0782 | 0.1569, 0.1460 | 0.1068, 0.1017 | 0.0872, 0.2409 | 0.1766, 0.1507 | 0.1758, 0.4035 |
| Largest diff. peak and hole (e.Å$^{-3}$) | 0.289, -0.310 | 0.153, -0.238 | 0.184, -0.186 | 0.228, -0.241 | 0.387, -0.709 | 0.187, -0.206 | 1.108, -0.504 |

**Thermogravimetric analysis – Differential scanning calorimetry (TGA-DSC).** Thermal analyses were carried out on a simultaneous thermogravimetric analysis (TGA) - differential scanning calorimetry/differential thermal analysis (heat flow DSC /DTA) system NETZSCH -STA 449 F1 Jupiter. The samples (4-7 mg) were placed in an alumina pan and measured at a scan speed of 10 °C min$^{-1}$ from ambient temperature to 250 °C under $N_2$ atmosphere as protective and purge gas (their respective flow velocities were 20 and 40 mL/min).

**Attenuated Total Reflection Fourier Transform Infrared spectroscopy (ATR-FT-IR).** Infrared spectra were recorded with a Jasco 4700LE spectrophotometer with attenuated total reflectance accessory. The scanning range was 4000 to 400 cm$^{-1}$ and at a resolution of 4.0 cm$^{-1}$.

## Computational Details

The calculations reported herein were performed using the Gaussian-09[41] program package and the B3LYP-D/def2-TZVP level of theory.[42-44] The X-ray coordinates have been used to estimate the interactions in the solid state. This methodology and functional have been successfully used before to evaluate similar interactions.[45-48] The interaction energies used in this work were computed as the difference between the energies of the isolated monomers and their assembly, unless otherwise noted. The interaction energies

were corrected by using the Boys–Bernardi counterpoise methodology to eliminate the basis set superposition error (BSSE).[49] The Bader's quantum theory of "Atoms in Molecules" (QTAIM) has been used to characterize the noncovalent interactions using the AIMall program.[50] The molecular electrostatic potential (MEP) surfaces have been obtained using the cube files generated using the Gaussian-09 software and the B3LYP-D/def2-TZVP wave-funcions. The 0.001 a.u. isosurface has been used as the best estimate of the van der Waals surface.

## RESULTS AND DISCUSSION

The structures of 9-ethyladenine and the carboxylic coformers used in this work for the preparation of new solid forms by liquid-assisted grinding and solution crystallizations are shown in Scheme 1. From the list, we have found that 9-ethyladenine forms salts with malonic, succinic and fumaric acids, the most acidic and shorter alkylic chain acids. However, it can also form cocrystals with succinic and fumaric acids and the longer aliphatic dicarboxylics such as glutaric and adipic acids. According to the widely used p$K_a$ rule, a $\Delta$p$K_a$ higher than 2-3 is significative for a salt formation; while a value lower than 0, will result for a cocrystal. The p$K_{a1}$ of the selected coformers are from 2.83 for malonic acid to 4.42 for adipic acid. In the case of 9-ethyladenine, its p$K_a$ is 4.2.[51] Therefore, the $\Delta$p$K_a$ for the most acidic coformers (malonic and fumaric acids) is between 0-2 and in this case, the p$K_a$ rule is inappropriate. For the other carboxylic acids, their p$K_a$ value is equal or lower than 0, suggesting that cocrystal forms should be expected. A recent study, carried out by A. J. Cruz-Cabeza, based on sufficient data from the Cambridge Structural Database, is in agreement with previous observations for the extreme values ($\Delta$p$K_a$ < -1 and $\Delta$p$K_a$ > 4). For the range in between -1 to 4, linear relationships have been found among the probability of salt ($P_{obs}$ ($A^-B^+$, %) = 17$\Delta$p$K_a$ +

28) or cocrystal ($P_{obs}$ (AB, %) = -17Δp$K_a$ + 72) formation and their Δp$K_a$.[52] Following both formulae, salt formation shows similar likehood for malonic and fumaric acid. However, for succinic, glutaric and adipic acids, the probability of obtaining cocrystals are higher (>70 %).

All these structures were solved by single-crystal X-ray diffraction and the bulk solids were further analysed by PXRD, FT-IR and thermal analysis. The noncovalent forces were studied by performing DFT calculations and also using the QTAIM computational tools in order to evaluate the contribution of individual H-bonding interactions to the binding energy of the assemblies.

**PXRD results.** The PXRD patterns of the novel crystalline multicomponent forms synthesized in this work are shown in the Supplementary Information (Figure S1) by overlays of the experimental pattern, the calculated pattern from the crystal structure and those of the starting materials. In all cases, the agreement between the experimental and the simulated patterns are good.

**Crystal structure analysis of salts and cocrystals of 9ETADE.** Evaporative crystallization methods were performed in an attempt to obtain regular and suitable single crystals for structural characterization by single crystal X-ray diffraction in each of the studied compounds.

*9-Ethyladenine-malonic acid (1:1) hydrated salt* (**1**). Compound **1** crystallizes in the triclinic P-1 space group containing one molecule of 9-ethyladenine, one of malonic acid and one of water in the asymmetric unit.

This structure presents pairs of 9-ethyladenine self-assembled through the Hoogsten edge N(6)-H···N(7) (2.982(3) Å, 161.8°) (black lines in Figure 1a). 9-ethyladenine interacts with hydrogenmalonate acid from one side through protonated N1 by N(1)-H···O(1)

(2.606(3) Å, 171.3°) and N(6)-H···O(2) (2.821(3) Å, 171.8°) interactions. But also, through a second one, bonding H2 and the carbonyl moiety of the carboxylate group by C(2)-H···O(1) (3.170(4) Å, 164.2°) (light blue lines in Figure 1a). Finally, the water molecule is bound to carboxylic groups of malonic acid, establishing three different hydrogen bonds: O(4)-H···O(5) (2.556(3) Å, 164.3°), O(5)-H···O(3) (2.798(3) Å, 170(4)°) and O(5)-H···O(2) (2.662(3) Å, 170(3)°) (green, purple and orange lines, respectively, in Figure 1a), acting as hydrogen bond donor and acceptor at the same time.

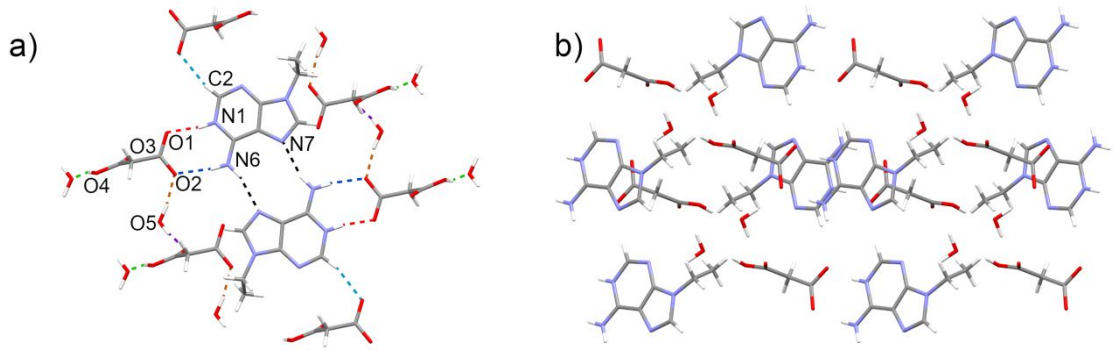


**Figure 1.** a) 9-ethyladenine– malonic acid hydrated salt dimer surrounded by their respective malonic acid and water molecules. b) Stacking of 9-ethyladenine– malonic acid hydrated salt (**1**).

Such adenine dimers form planes in association with other neighbor dimers through the hydrogenmalonate acid and water molecules. Then, those planes stack on top of each other. In every dimer, a salt bridge between 9-ethyladenine and malonic acid molecules interacts with the one below and the other with the one above, through π-π stacking (π-π interplanar distance 3.404 Å). Water molecules establish additional hydrogen bonds with neighbor malonic acid molecules (see Figure 1b).

*9-Ethyladenine-succinic acid (1:1) salt* (**2**). 9-ethyladenine– succinic acid salt crystallizes in the triclinic P-1 space group containing a protonated molecule of 9-ethyladenine, half succinic acid and half succinate molecules in the asymmetric unit.

This structure is formed by infinite chains of alternating succinate and succinic acid molecules connected through O(30)-H···O(20) (2.5466(16) Å, 179.3(19)°) hydrogen bonds. Those chains form planes by π-π stacking of succinate molecules (π-π interplanar distance 3.218 Å).

9-ethyladenine forms also planes. First by dimeric units by N(6)-H···N(7) (2.914(2) Å, 159.9(18)°) (red lines in Figure 2a) and secondly forming π-π stacking of nitrogenous bases (π-π interplanar distance 3.406 Å). Finally, those dimers also interact through their hydrophobic chains forming planes of 9-ethyladenine.

Succinate/succinic acid planes and 9-ethyladenine planes are then linked together, establishing hydrogen bonds between non self-assembling nitrogen atoms of adenine and succinate molecules through N(1)-H···O(20) (2.6852(19) Å, 165.1(17)°) and N(6)-H···O(21) (2.760(2) Å, 162.9(18)°) interactions (green and purple lines respectively in Figure 2a). Therefore, the whole structure can be defined as alternating layered planes of 9-ethyladenine and succinate/succinic acid (see Figure 2b).

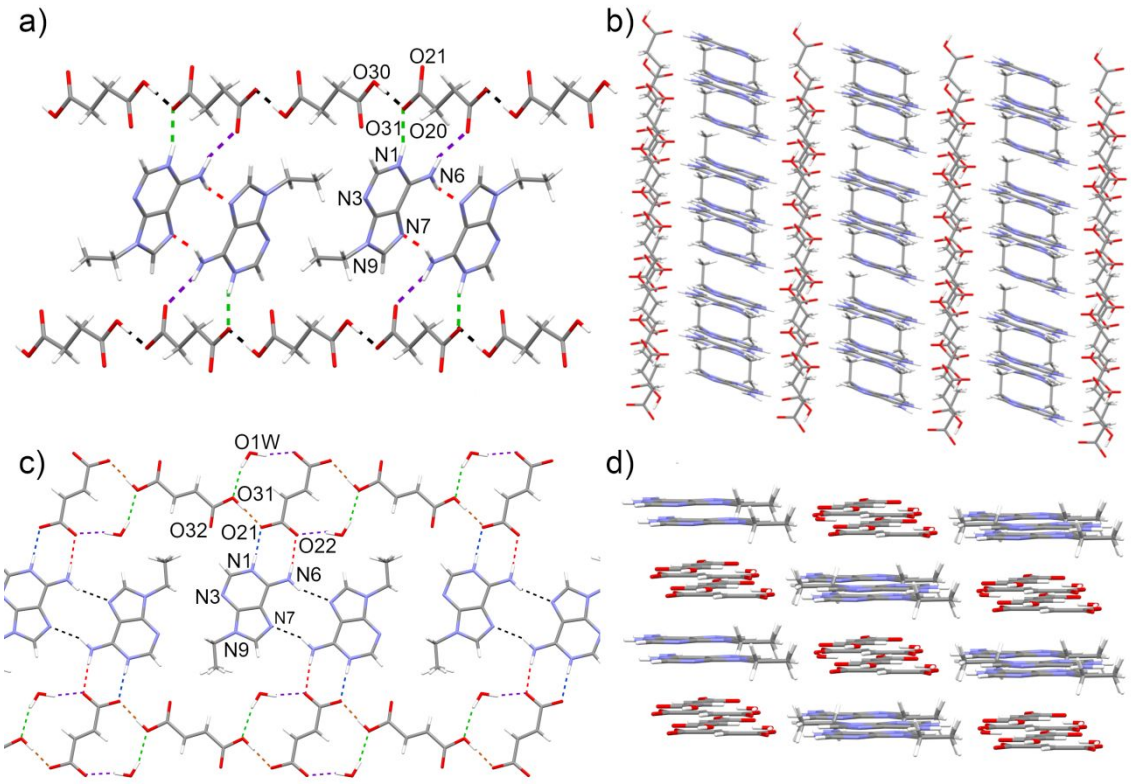


**Figure 2.** a) 9-ethyladenine– succinic acid salt (**2**) interactions between layers along the **a** axis. b) Layers of 9-ethyladenine– succinic acid. c) 9-ethyladenine– fumaric acid salt (**5**) planes. d) Stacking of 9-ethyladenine– fumaric acid salt planes.

This structure presents many similarities with 9-ethyladenine– malonic acid hydrated salt. Its self-assembling arrangement is performed through the same side of 9-ethyladenine, other nitrogen atoms are free to bind to the acid group of the selected molecule and π-π assembling plays a major role between 9-ethyladenine dimers.

*9-Ethyladenine-succinic acid (2:1) cocrystal* (**3**) and *9-Ethyladenine-Fumaric acid (2:1) cocrystal* (**6**). Both structures are almost identical. Surprisingly, the restriction caused by a double bond in fumaric acid compared to succinic acid has very small influence. Proportions, arrangement and even distances and angles of hydrogen bonds formed are very similar. Both cocrystals crystallize in the monoclinic $P2_1/n$ space group, where the cell for compound **3** is half the one of the compound **6** (the two adenines are named A

and B and present the same hydrogen bond pattern with different bond distances and angles).

These structures present a particular self-assembling arrangement for 9-ethyladenine that is different to the one described for previous structures. In these cases, N6 binds at the same time with N1 and N7 through the following hydrogen bonds: a) for compound **3**, N(6)-H···N(1) (3.055(4) Å, 165.6°) and N(6)-H···N(7) (3.044(4) Å, 174.5°) (red and black lines, respectively, in Figure 3a); b) for compound **6**, N(6A)-H···N(1A) (3.091(4) Å, 163(3)°), N(6B)-H···N(1B) (3.115(4) Å, 165(3)°), N(6A)-H···N(7A) (3.059(4) Å, 174(3)°) and N(6B)-H···N(7B) (3.047(4) Å, 175(3)°) (red and black lines respectively in Figure 3c). Therefore, they are connected to the adjacent adenines through both Watson-Crick and Hoogsten edges, forming infinite zig-zag tapes of the modified nucleobase (for **6**, the tapes are formed exclusively with adenine A or adenine B). These tapes are then connected to: a) for compound **3**, succinic acid molecules through O(2)-H···N(3) (2.664(3) Å, 167.2°) (blue lines in Figure 3a), giving rise to a plane in which tapes are faced in opposing directions; b) for compound **6**, fumaric acid molecules through O(2)-H···N(3A) (2.658(4) Å, 169(5)°) and O(3)-H···N(3B) (2.647(4) Å, 169(4)°) interactions (blue lines in Figure 3c), with the chains placed in opposite directions, alternating A and B chains, and forming parallel layers (as can be seen in Figure 3d).

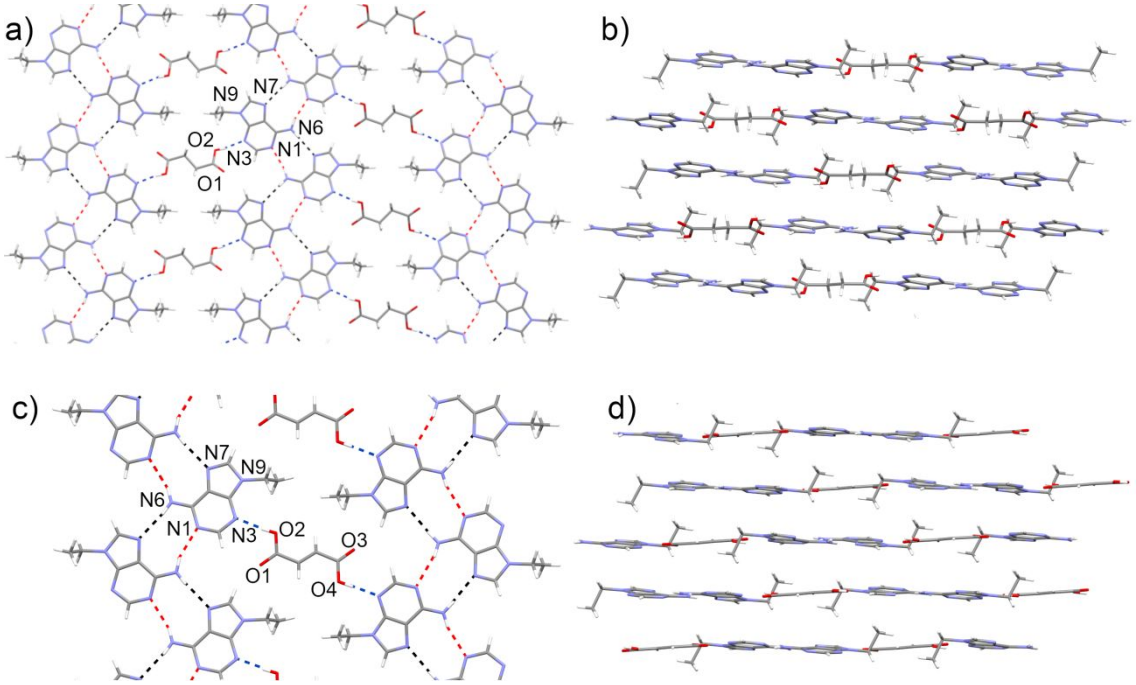


**Figure 3.** a) Zig-zag tapes in 9-ethyladenine– succinic acid cocrystal (**3**). b) Crystal packing of 9-ethyladenine– succinic acid planes. c) Zig-zag tapes in 9-ethyladenine–fumaric acid cocrystal (**6**). d) Stacking of 9-ethyladenine– fumaric acid cocrystal.

For compound **3**, such planes are pilled through a cluster of aromatic interactions (Figure 3b). In the center of the cluster, 9-ethyladenine stacks in pairs (π-π interplanar distance 3.434 Å). At both sides of this pair, a carbonyl establishes a lone pair interaction with the aromatic system of 9-ethyladenine (O(1)···Centroid distance: 3.505 Å, angle 95.23°). At the outer sphere of the cluster, this carbonyl interacts with another adenine (O(1)···N(1): 3.698 Å, angle 69.83°) and the hydroxyl group interacts with a second neighbor adenine (O(2)···N(6): 3.430 Å, angle 111.39°). On the other hand, for compound **6**, the planes are placed on top of one another by π-π stacking of nitrogenous bases, specially visible with the five-membered rings (N(9A)···Centroid distance: 3.348 Å, N(9B)···Centroid distance: 3.351 Å) (Figure 3d).

All these new arrangements suggest that the addition of a carbon atom in the carboxylic molecule induces an increased influence of the Van der Waals forces. For this structure, 9-ethyladenine molecules are accommodated to face their alkylic chains all in the same direction as the acid molecules. These zig-zag tapes have been previously described. They are formed by *trans* Watson-Crick/Hoogsteen base pairs, which compared to *trans* Watson-Crick/Watson-Crick are somewhat higher in energy but occur more frequently.[53-54]

*9-Ethyladenine-Glutaric acid (1:1) cocrystal* (**4**) and *9-Ethyladenine-Adipic acid (1:1) cocrystal* (**7**). Both cocrystals present very similar structures, crystallizing in the monoclinic $P2_1/c$ space group, where the cell for compound **4** is half the one for compound **7**. In compound **7**, the two adipic molecules in the asymmetric unit posses three protonated sites, which corresponds to a cocrystal/salt mixture. However, given the difficulties found in the determination of the crystal structure of **7**, the position of the protons in the O···N hydrogen bonds is dubious, hence its assignation to salt or cocrystal.

These structures form planes perpendicular to the *c* axis (for **4**) or parallel to the *b* axis (for **7**). 9-ethyladenine interacts with glutaric acid in two different ways. First, through its Watson-Crick edge, establishing hydrogen bonds both as a donor and an acceptor by: a) for compound **4**, O(21)-H···N(1) (2.673(2) Å, 167(2)°) and N(6)-H···O(22) (2.925(2) Å, 169.9°) interactions (red and blue lines respectively in Figure 4); b) for compound **7,** O(1C)-H···N(1A) (2.669(4)Å; 167(6)°) and N(6A)-H···O(2C) (2.976(4) Å; 170.6°) and O(1D)-H···N(1B) (2.642(4) Å; 156(6)°) and N(6B)-H···O(2D) (2.947(5) Å; 169.7°). Then, through its Hoogsteen edge also establishes hydrogen bonds both as donor and acceptor by: a) for compound **4**, N(6)-H···O(26) (2.868(2) Å, 171.8°) and O(27)-H···N(7) (2.658(2) Å, 169(2)°) (purple and orange lines respectively in Figure 4a); b) for compound **7**, N(6B)-H···O(7C) (2.843(5) Å; 168.7°) and O(8C)-H···N(7B) (2.719(4) Å; 163(6)°)

and as double donor by N(6A)-H···O(7D) (2.846(4) Å; 171.4°) and N(7A)-H···O(8D) (2.714(4) Å; 166(4)°) (see Figure 4c). Moreover, in compound **4**, 9-ethyladenine establishes hydrogen bonds with its nearest neighbor by C(2)-H···N(3) (3.361(3) Å, angle 147.2°) (black lines in Figure 4a).

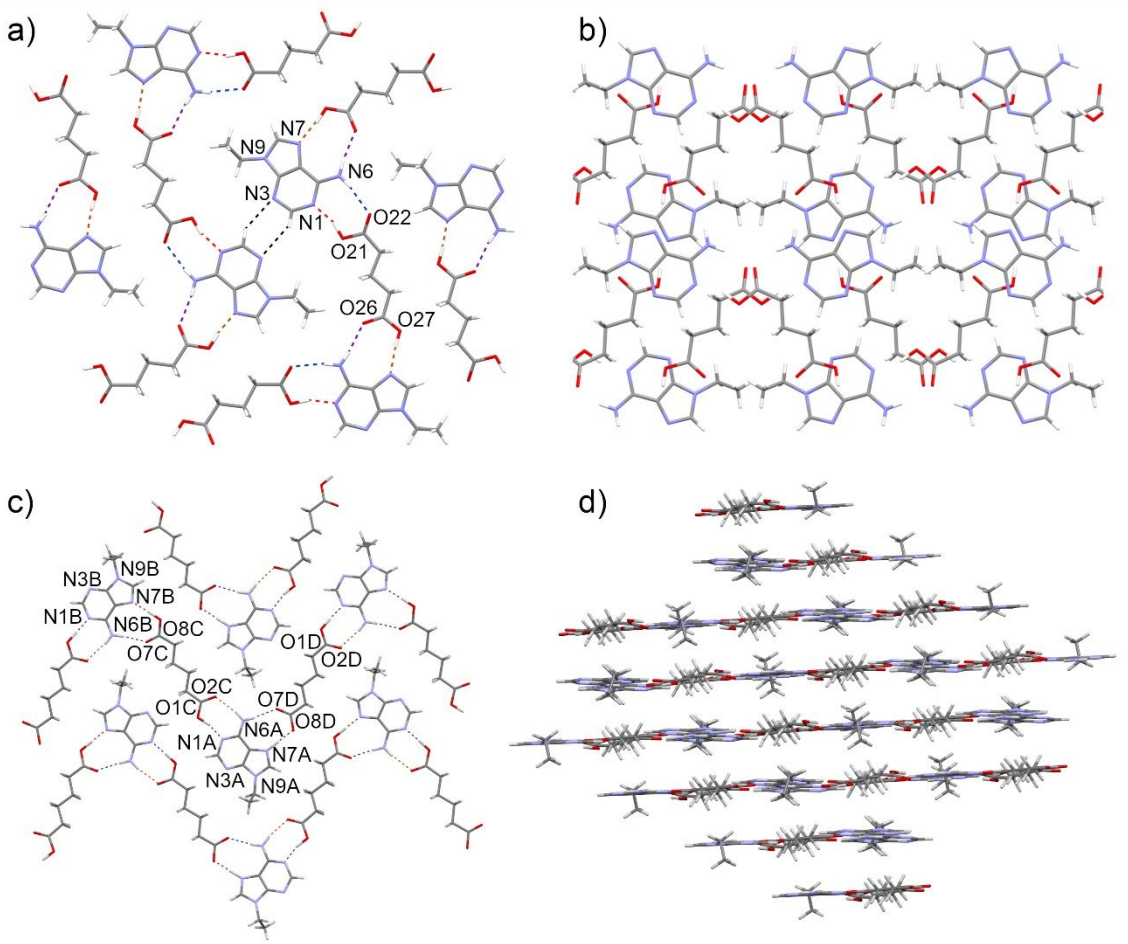


**Figure 4.** a) 9-ethyladenine– glutaric acid cocrystal (**4**) planes. b) π-π stacking of 9-ethyladenine– glutaric acid cocrystal planes. c) 9-ethyladenine– adipic acid cocrystal (**7**) planes. d) Stacking of 9-ethyladenine– adipic acid cocrystal planes.

In compound **4**, the planes establish π-π stacking interactions among 9-ethyladenine molecules (π-π interplanar distance 3.366 Å), but also π-π stacking between carboxylic

groups and 9-ethyladenine by O(27)···N(3) (3.459 Å, angle 77.57°) as shown in Figure 4b.

Regarding compound **7**, the planes overlap due to weak van der Waals interactions among adenines and adipic acid molecules, i.e. long C-H···π /C-H···O bonds. The weakness of the interplane interactions explain the high mosaicity of the crystal along **a*** (see Figure 4d).

In comparison with other multicomponent forms of 9-ethyladenine, it appears that the increasing length of the linear alkylic dicarboxylic acid in compounds **4** or **7** causes adenines to be further apart from one another, preventing them from establishing a canonical self-assembled arrangement through their Watson-Crick or Hoogsteen edges, such as those seen in previous structures; but even also, in the case of compound **7,** from any other type of interaction, like to observed in **4** among C(2)-H···N(3)**.**

The adenine arrangement found in compound **4** constitutes an alternative adenine-adenine self-assembled motif not found in DNA nor RNA (up to the authors' knowledge), although it has been previously described by others[55] and several structures are deposited at the CCDC showing such pattern.[56-62]

*9-Ethyladenine-Fumaric acid (1:1) hydrated salt* (**5**). This salt crystallizes in the monoclinic C2/m space group containing one molecule of 9-ethyladenine, half of a fumaric acid, half of a fumarate and one molecule of water in the asymmetric unit.

This structure presents also a self-assembled arrangement between adenines through the Hoogsten edge: N(6)- H···N(7) (2.966(5) Å, 158.6°) (black lines in Figure 2c). Adenine dimers are only bound to fumarate molecules by two interactions: N(1)-H···O(21) (2.711(4) Å, 179(5)°) and N(6)-H···O(22) (2.793(5) Å, 175.4°) (blue and red lines, respectively, in Figure 2c). These units are then connected to their neighbors through

fumaric acid thanks to hydrogen bonds O(31)-H···O(21) (2.550(4) Å, 179(5)°) (orange lines in Figure 2c). Furthermore, water molecules act as bridges between fumarate and fumaric acid molecules (O(1W)-H···O(22), 2.790(6) Å, angle 167(9)° and O(1W)-H···O(31), 2.974(7) Å, angle 166(9)°) (purple and green lines, respectively, in Figure 2c).

Layers are piled up by π-π stacking of 9-ethyladenine and fumaric acid molecules. In this structure, molecules lay perfectly flat in relation to one another base (π-π interplanar distance 3.263 Å). Such stacking is shown in Figure 2d.

Compared to the structures of succinic and fumaric acid cocrystals with 9-ethyladenine, this structure presents also chains of acid molecules and chains of 9-ethyladenine, but in this case adenine does not form infinite zig-zag tapes. Similarities can be found respect to 9-ethyladenine-succinic acid salt; in both cases infinite chains of carboxylic acids are found and adenine forms also dimers. However, the final packing is different, for the succinic acid salt there are alternated columns of succinic acids and 9-ethyladenines while for the fumaric acid salt, the columns are formed by alternated fumaric acids and 9-ethyladenines.

**Thermal analysis.** The thermal stability of the resulting salts and cocrystals of 9-ethyladenine was examined by TGA-DSC (Figures S2). In Table 2, a summary with the melting points of the starting compounds and the synthesized multicomponent forms is collected.

**Table 2.** Melting points of 9-ethyladenine salts and cocrystals.

| Compound | mp (°C) | coformer | mp (°C)** |
|---|---|---|---|

| | | | |
|---|---|---|---|
| 9-ethyladenine | 191 | | |
| **1** | 72* | Malonic acid | 132-135 |
| **2** | 191.5 | Succinic acid | 185-191 |
| **3** | 199.6 | | |
| **4** | 207.5 | Glutaric acid | 95-98 |
| **5** | 226.3 | Fumaric acid | 298-300 |
| **6** | 224.1 | | |
| **7** | 157.5 | Adipic acid | 151-154 |

*dehydratation event. **Sigma-Aldrich.

The melting point of 9-ethyladenine was observed at 191 ºC in the DSC trace, in agreement with literature.[63]

The thermal analysis of the salt **1** showed a weight loss (ca. 5.8 %) between room temperature and 100 ºC, associated to the complete dehydration of the sample (theor. LOD: 6.3 % for one molecule of water). This event is associated with an endothermic peak with an onset ($T_o$) and melting ($T_m$) temperatures of 52 and 72 ºC, respectively, in the DSC. A second endothermic peak at 140 °C ($T_o$) is observed corresponding to the melting of the compound. The combination of 9-ethyladenine and succinic acid has afforded two multicomponent solid forms, a salt (**2**) and a co-crystal (**3**). Both forms are anhydrous according to their TGA traces and their melting points are in both cases similar to the nucleobase but higher than the one of succinic acid. Use of fumaric acid as coformer also afforded two crystalline solid forms: a hydrated salt (**5**) and an anhydrous cocrystal (**6**). In both cases, their melting points are similar with a value in between the melting points of 9-ethyladenine and the fumaric acid precursor. The resulting cocrystal **4**, formed from 9-ethyladenine and glutaric acid, was anhydrous and showed a melting point higher than its precursors, which means that the obtained crystalline form exhibits a higher stability. Cocrystal **7** corresponds to the pair between 9-ethyladenine and adipic acid

molecules. This solid form is anhydrous and has a melting point ($T_m$) of 158 ºC, also a value in between of that of its pure components.

**FT-IR Spectroscopy.** The FTIR spectra of the new solids were compared with those of the corresponding pure components (Figure S3, included in Supplementary Materials). Although in some cases, specially for cocrystals, it might seem that the resulting spectra are just the sum of the parent compounds, a detailed analysis shows that there are a few differences which help to confirm the creation of the new forms. For instance, for the 9-ethyladenine-malonic acid hydrated salt (**1**), a new band at 3447 $cm^{-1}$ appears, which could be assigned to O-H stretching from a water molecule. Moreover, in the middle region frequencies, there is a shift for the carbonyl band from the carboxylic group from 1691 $cm^{-1}$ (in free malonic acid) to 1696 $cm^{-1}$ for this salt, as a result of overlapping with C=N and C=C stretchings. This blue shift in the C=O band was also observed for the 9-ethyladenine– succinic acid salt (1:1) (from 1679 to 1702 $cm^{-1}$) and the 9-ethyladenine–fumaric acid hydrated salt (1:1:1), from 1656 to 1710 $cm^{-1}$. For the latter, water (O-H) was also confirmed by the presence of new bands at 3588 and 3407 $cm^{-1}$. All cocrystals forms show similar FTIR spectra with two characteristic bands between 3115 and 3330 $cm^{-1}$ for the N-H and C-H stretchings, at higher frequencies respect to the 9-ethyladenine. Moreover, there is a new band around 1857-1914 $cm^{-1}$ which can be assigned to the ν(O-H) (OH···N) according to the literature.[64-65] And finally, three bands are observed in the region of the C=N, C=C and C=O stretchings, slightly blue-shifted regarding to 9-ethyladenine but, in general, at lower frequencies than for the corresponding free acids.

**Theoretical calculations.** The theoretical study is devoted to analyze several supramolecular assemblies observed in the solid state of the co-crystals and to assign individual energies to the different H-bonding interactions and unconventional π-stacking

complexes. This type of analysis is convenient to understand the different combinations of interactions and also to give insight into the ability of the Hoogsteen and Watson-Crick faces of neutral and protonated adenine to participate in H-bonding networks with itself (self-assembly) and/or carboxylic/carboxylate groups.

For compound **1**, the unconventional π–π stacking interactions that involve the salt bridges (highlighted in Figure 5) were first analyzed. As explained above, the adenine ring is protonated in N1 and forms a salt bridge complex with hydrogen malonate. The formation energy of this salt bridge is very large (–109.3 kcal/mol, see Figure 5a) due to the large contribution of the electrostatic attraction between the opposite charges. In Figure 5, the QTAIM distribution of critical points (CPs) and bond paths is represented for the salt bridge (a) and its stacked assembly (b). The salt bridge interaction is characterized by two bond CPs (green spheres) and bond paths connecting the O-atoms to the H-atoms. The individual energetic contribution of each hydrogen bond was calculated using the kinetic energy $G(r_{CP})$ value at the bond critical point (values in black in Figure 5). Thus, the energy for each H-bond was calculated according to the approach by Vener *et al*.[66] (see values in red in Figure 5) that was explicitly developed for hydrogen bonding interactions [Energy = 0.429 * G(r)]. For pure closed-shell H-bonds, this proportionality is equivalent to that with the parallel curvature of the electron density $\lambda_3(r_{CP})$, as $G(r_{CP})$ is linearly related with $\lambda_3(r_{CP})$.[68-69] The QTAIM results indicate that the H-bonding contribution to the salt-bridge formation is 16.8 kcal/mol and the rest is due to the pure electrostatic atraction. Figure 5b shows the interesting salt-bridge···salt-bridge (SB···SB) stacking where the salt-bridges are arranged in an anti-parallel mode to maximize the electrostatic atraction. The AIM distribution of CPs and bond paths reveals that the assembly is characterized by four CPs and bond paths interconnecting the O and N atoms. The interaction is further characterized by the presence of several ring (in yellow) and cage (in blue) CPs. In addition, the assembly is also estabilized by two

symmetrically equivalent C–H···π interactions characterized by a bond CP and bond path connecting a H-atom of hydrogen malonate to the N-atom of the five-membered ring of adenine. The interaction energy of the SB···SB stacking interaction is large –22.4 kcal/mol, thus confirming the importance of this synthon in the solid state structure of **1**.

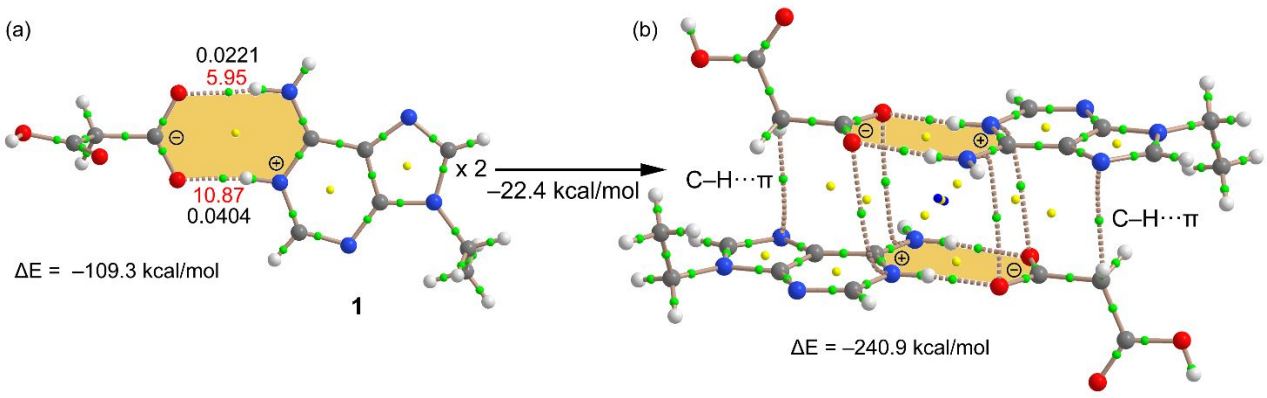


**Figure 5.** QTAIM distribution of bond, ring and cage CPs (green, yellow and blue spheres, respectively) in two assemblies of compound **1**; dimer (a) and tetramer (b). The G(r) values at selected bond CPs are given using a black font and the dissociation energy of the H-bonds using a red font (in kcal/mol). The formation energies (ΔE) computed at the B3LYP-D/def2-TZVP level of theory are also indicated.

In addition to the SB···SB interaction, compound **1** also forms self-assembled H-bonded dimers in the solid state through the Hoogsten side of adenine (see Figure 6). Each N6-H···N7 H-bond contributes in 3.58 kcal/mol, thus being weaker than any of the N–H···O bonds. It is worth mentioning that the formation energy of the H-bonding dimer represented in Figure 6b considering the salt-bridge as monomer is –14.0 kcal/mol. This dimerization energy is significantly smaller (in absolute value) than the SB···SB dimer formation (–22.4 kcal/mol, see Figure 6), thus indicating that the latter has a larger influence in the solid state of compound **1**. It should be mentioned the large difference between the dimerization energy (–14.0 kcal/mol) and the sum of the H-bond dissociation energies predicted using the QTAIM parameters (7.16 kcal/mol). This is due to the fact

that the pure electrostatic attraction between the counterions (9-ethyladeninium and malonate) are not taken into consideration when the QTAIM energy predictor is applied. Therefore, approximately half of the dimerization energy is due to electrostatic effects and the other half to to the contribution of both N–H···N H-bonds.

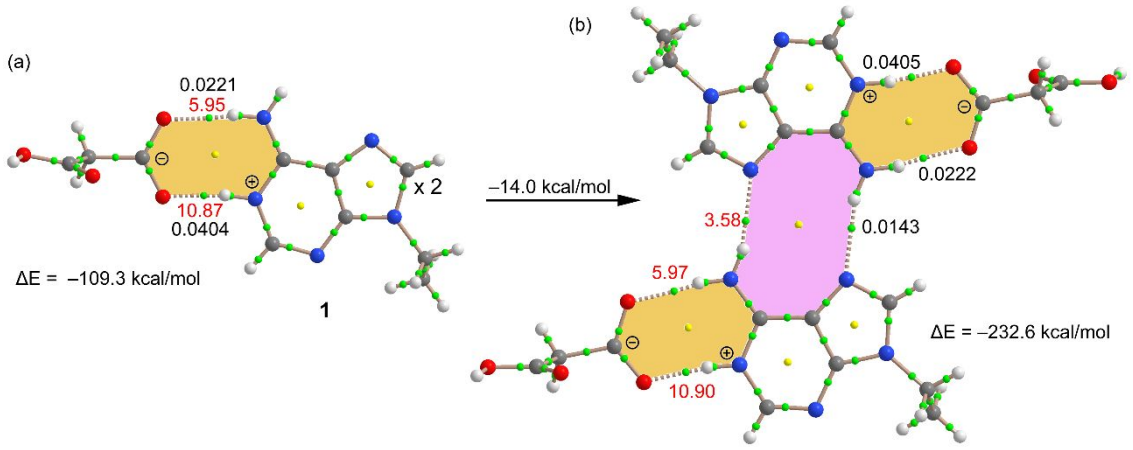


**Figure 6.** QTAIM distribution of bond, ring and cage CPs (green, yellow and blue spheres, respectively) in two assemblies of compound **1**; dimer (a) and tetramer (b). The G(r) values at selected bond CPs are given using a black font and the dissociation energy of the H-bonds using a red font (in kcal/mol). The formation energies (ΔE) computed at the B3LYP-D/def2-TZVP level of theory are also indicated.

The adenine ring is neutral in compounds **3** and **6** and, consequently, these compounds are adequate to analyze possible competition between the Watson-Crick and Hoogsten faces of the adenine ring for the formation of H-bonding complexes. First of all, the molecular electrostatic potential (MEP) surface of 9-ethyladenine has been obtained, in order to know the relative ability of H-bond donor and acceptor sites (see Figure 7). The MEP analysis reveals that N1 is the best H-bond acceptor and N3 and N7 are very similar. Regarding the H-bond donor, the MEP values are equivalent at both H-atoms of the exocyclic $–NH_2$ group. This suggests that both faces of adenine are equivalent as H-bond

donor and that the Watson-Crick face is better H-bond acceptor. In Figure 7b the MEP surface has been represented using a different scale in order to show the π-electronic difference between the six and five membered rings. Although the MEP values over the ring centers are very small, it is negative over the six membered ring and positive over the five membered ring. Therefore, from an electrostatic point of view, the latter is adequate for interacting with electron rich atoms.

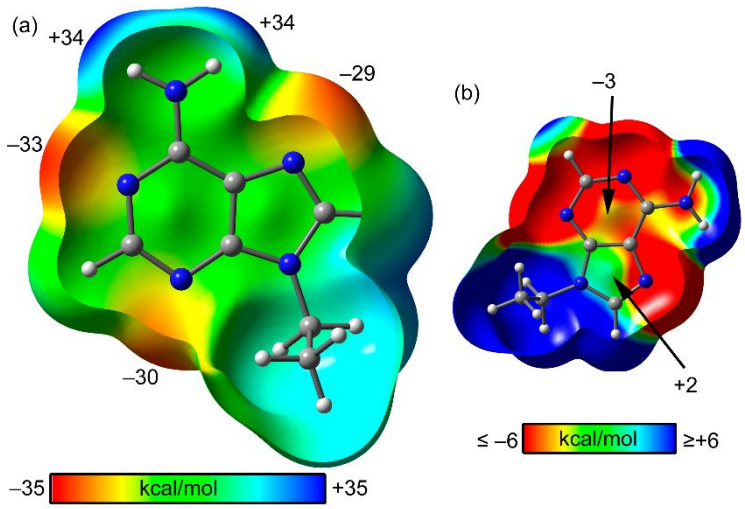


**Figure 7**. (a,b) Open molecular electrostatic potential (MEP) surface of 9-ethyladenine using two different scales. The energies at selected points of the surface are indicated in kcal/mol.

Both compounds **3** and **6** form similar H-bonding networks in the solid state as represented in Figure 8. Both adenine faces interact with adjacent adenines forming two sets of N6–H6A···N1 and N6–H6B···N7 H-bonds. The energies associated to these H-bonds (from QTAIM) are indicated using a red font in the figure. They range from 2.99 to 3.47 kcal/mol. In both compounds the carboxylic acid (succinic acid in **3** and fumaric acid in **6**) forms a strong H-bond interaction with N3. In both compounds the O-atom that participates in the O–H···N3 H-bond also establishes a bifurcated H-bond (as acceptor) with the 9-ethyl substituent. Finally, in case of fumaric acid, a weak C2–H···O H-bond is

also established (1.35 kcal/mol). The total formation energy (from QTAIM) is similar for both compounds and also comparable to the formation energy obtained from DFT calculations (ΔE = –28.7 kcal/mol), thus giving reliability to the QTAIM estimation of individual energies.

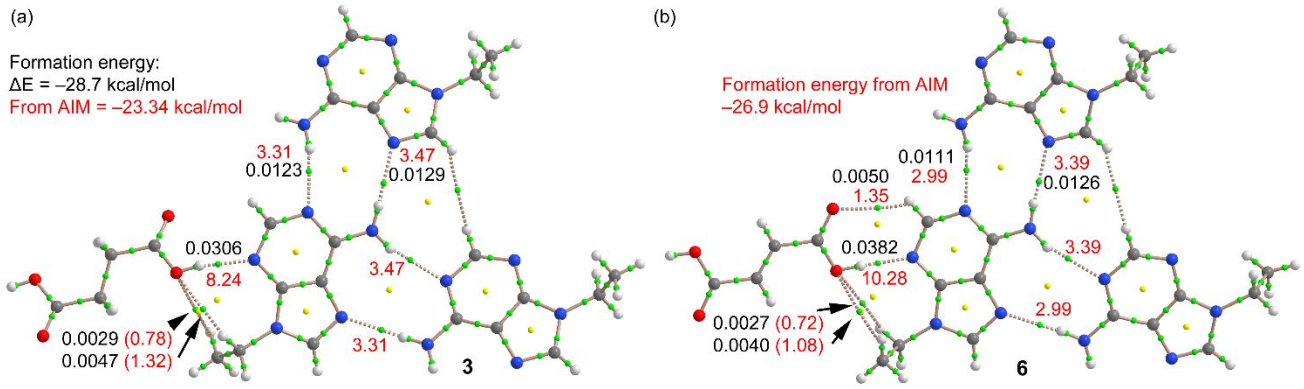


**Figure 8**. QTAIM distribution of bond, ring and cage CPs (green, yellow and blue spheres, respectively) in the H-bonding network of compound **3** (a) and **6** (b). The G(r) values at selected bond CPs are given using a black font and the dissociation energy of the H-bonds using a red font (in kcal/mol). The formation energies (ΔE) computed at the B3LYP-D/def2-TZVP level of theory are also indicated in black. Those estimated from QTAIM in red.

As commented above, the main difference between the crystal packing of compound **3** and **6** is the existence of an additional H-bonding interaction, C2–H···O interaction in **6** between the fumaric acid and adenine. In compound **3,** the H···O distance is longer because the O atom is tilted toward the five membered ring of an adenine molecule from an adjacent 2D layer forming a lp–π interaction (ΔE = –5.2 kcal/mol, see Figure 9a), in line with the MEP surface analysis. We have also evaluated the assembly considering the H-bonding network described in Figure 8, and the interaction energy increases to ΔE = –8.9 kcal/mol, see Figure 9b. The QTAIM analysis indicates that the lp–π interaction is characterized by two bond CPs and bond paths that connect the O-atom to two atoms of

the five membered ring, thus confirming the existence of the interaction. The AIM analysis also reveals an intricate combination of bond CPs and bond paths connecting the succinic acid to the adenine rings. Moreover, it also reveals the existence of interaction between the O-atom and an H-atom of the ethyl group. In order to estimate the contribution of the lp–π interaction, a modified model of the complex used in Figure 9a has been used, where the ethyl group has been mutated to a methyl group, and consequently this ancillary interaction is not formed. As a result, the interaction energy is slightly reduced to ΔE(Et→Me) = –4.8 kcal/mol, which can be attributed exclusively to the lp–π interaction.

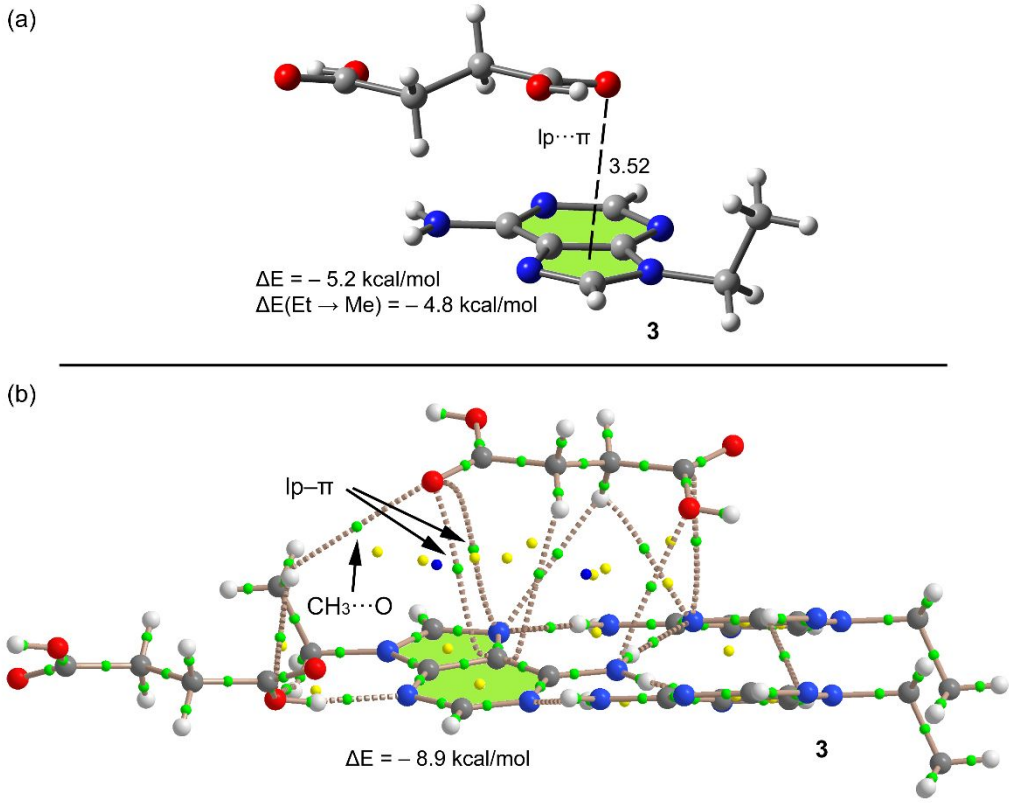


**Figure 9**. (a) Lp–π complex observed in the solid state of compound **3** and its interaction energy using two models (see main text). Distance in Å. (b) QTAIM distribution of bond, ring and cage CPs (green, yellow and blue spheres, respectively) in the H-bonding network of compound **3** interacting with succinic acid.

The structure of compound **4** is interesting because the glutaric acid interacts with both faces of adenine ring, so it is adequate to compare both binding modes and also can be considered as a minimalistic model of the interaction of adenine with the side chain of aminoacids like glutamic or aspartic. The QTAIM analysis of the H-bonding network oberved in **4** is shown in Figure 10. The interaction via the Watson-Crick face obtained from the QTAIM analysis is 14.79 kcal/mol that is slightly less favored than the interaction via the Hoogsten face (15.66 kcal/mol). It is interesting to highlight that the N–H···O hydrogen bonds are significantly weaker than the O–H···N bonds in line with the aditity of the H-bond donor and the basicity of the acceptor. Finally, the adenine ring interacts with the adjacent adenine through weak C2–H···N3 hydrogen bonds (1.75 kcal/mol).

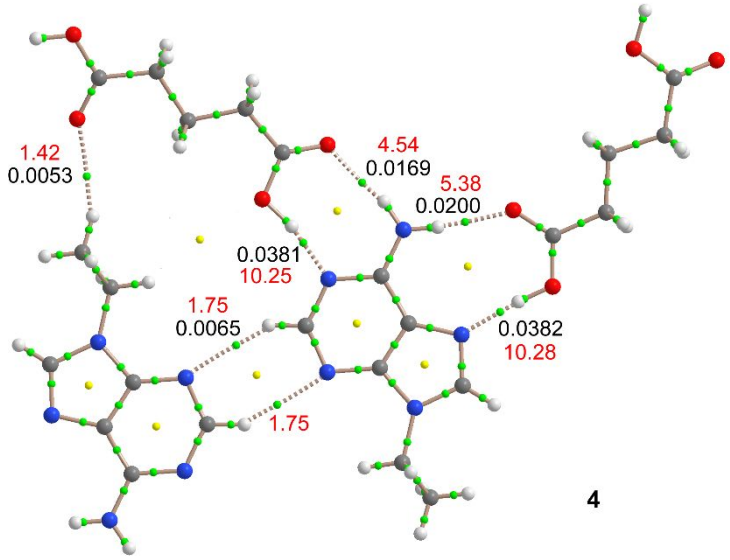


**Figure 10**. QTAIM distribution of bond, ring and cage CPs (green, yellow and blue spheres, respectively) in the H-bonding network of compound **4**. The G(r) values at selected bond CPs are given using a black font and the dissociation energy of the H-bonds using a red font (in kcal/mol).

Finally, in compound **5** the self-assembled dimer that is formed by the interaction of two protonated adenine rings (see Figure 11) through the Hoogsten face has been analyzed. This dimer is formed against the electrostatic repulsion of two cationic species ($N^9$-ethyladeninium). Therefore, the symmetrically equivalent N6–H···N7 H-bonds can be considered as examples of the so-called "anti-electrostatic H-bonds" (AEHBs).[69] It has been demonstrated that, in spite of the ionic repulsion, the properties of the hydrogen bonds remain the same in neutral and charged systems.[70] In fact, aggregates of molecules of the same charge are frequently reported in crystal structures[71-73] where the surrounding counterions balance the ionic repulsion. These aggregates can be stable in gas phases, as it has been shown that hydrogen bonds can overcome ionic forces in some cases.[74] For the adenine dimer of compound **5** (dicationic complex) the energy is positive ($\Delta E$ = +30 kcal/mol). However, the individual interaction energies measured from the QTAIM are favorable (dissociation energy = 4.03 kcal/mol for each H-bond). As the dissociation energy includes a positive contribution from cation-cation repulsion and a negative contribution from the hydrogen bonds, it is clear that the first one is more important. This does not preclude that the dimer is stable, but that the dimer corresponds to a local energy minimum, as dimers formed by two protonated nucleobases have been shown to be stable in gas phase in spite of presenting positive dissociation energy.[75]

In case the counter-anions are included in the calculations (see Figure 11b), the dimerization energy becomes negative ($\Delta E$ = –18.3 kcal/mol) due to the presence of the dianions. Quite remarkably, the energy of the N6–H···N7 H-bonds in the assembly where the counterions are present is almost identical (4.06 kcal/mol) to those in the dicationic dimer. This is an expected result, as the presence of the counterions balances ionic repulsion, leaving the hydrogen bond as the main contribution to the dissociation energy.[76] This result confirms that hydrogen bonds in neutral or charged systems are extremely similar.

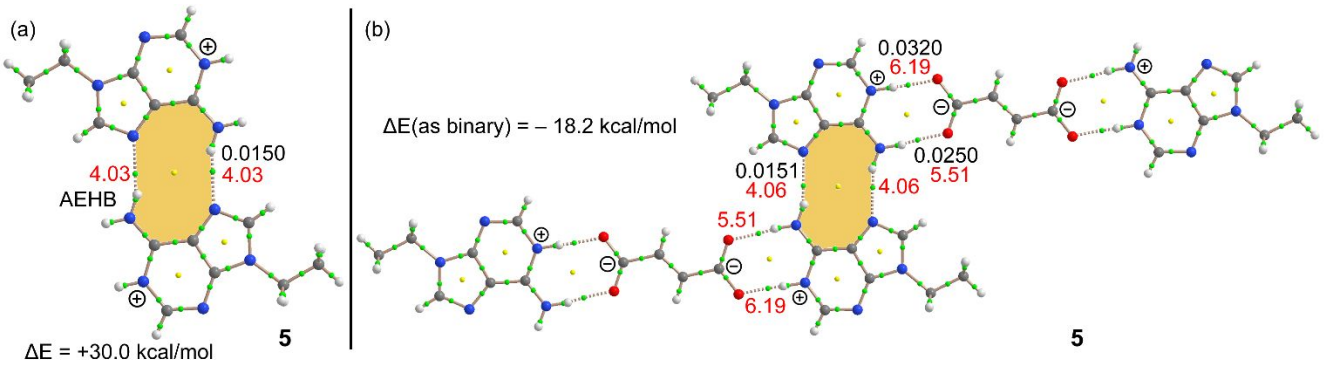


**Figure 11**. QTAIM distribution of bond and ring CPs (green and yellow spheres, respectively) in two assemblies of compound **5**; cation-cation dimer (a) and a neutral hexamer (b). The G(r) values at selected bond CPs are given using a black font and the dissociation energy of the H-bonds using a red font (in kcal/mol). The formation energies (ΔE) computed at the B3LYP-D/def2-TZVP level of theory are also indicated. In case of the assembly in (b) the energy has been computed as a dimerization of two trimers (only the N6–H···N7 H-bonds are evaluated)

## CONCLUSIONS

In conclusion, we have reported the synthesis of a new series of cocrystals and salts combining 9-ethyladenine and carboxylic acids with different alkylic chain lenght. The solids have been further characterized by different techniques including X-ray diffraction, spectroscopic techniques and thermal analysis. Through a careful analysis of the single crystal structures for all of them we have established the main interactions involved in the crystal packing. The obtained new salts with 9-ethyladenine form dimers. While for the cocrystals with succinic and fumaric acids zig-zag tapes of nucleobase molecules were observed; for glutaric and adipic acids, the addition of methylenes groups to the chain prevents from their canonical self-assembly.

The relationship between the salt/cocrystal form, the coformer used or even the length of the alkylic chain has been studied through DFT calculations by comparing the resulting interaction energies. They indicate that the H-bonds between carboxylic/carboxylate groups and adenine/adeninium rings (N–H···O and O–H···N) are stronger than those between adenines (N–H···N). The interaction energies through the Watson-Crick and Hoogsten faces with carboxylic groups are similar. In compound **1** the SB···SB interaction has been studied as it is energetically very relevant to the antiparallel arrangement of the salt bridges. In compound **3**, the lp–π interaction involving the five-membered ring has been investigated, demostrating by the MEP surface analysis that it is π-acidic. Finally, it has been shown that the so-called AEHBs between two adeninium moieties are basically identical to neutral HBs and that these HBs account for the dissociation energy when counteranions are included.

## Supporting Information

The Supporting Information is available free of charge on the ACS Publications website at DOI:

Additional information concerning XRD patterns, FT-IR spectra, TGA-DSC thermograms and Hydrogen-bond interactions of the new compounds.

CCDC numbers 1958269 - 1958275 contain the supplementary crystallographic data for this paper. These data can be obtained free of charge via www.ccdc.cam.ac.uk/data_request/cif, or by emailing data_request@ccdc.cam.ac.uk, or by contacting The Cambridge Crystallographic Data Centre, 12 Union Road, Cambridge CB2 1EZ, UK; fax: +44 1223 336033.

## AUTHOR INFORMATION


### Corresponding Authors

*Email: toni.frontera@uib.es

*Email: elies.molins@icmab.es

ORCID

Antonio Frontera: 0000-0001-7840-2139

Elies Molins: 0000-0003-1012-0551


### Author Contributions

All authors have given approval to the final version of the manuscript.


### Funding Sources

This research was funded by MINECO/AEI from Spain, project numbers ENE2015-63969, CTQ2017-85821-R FEDER and SEV2015-0496 and by the Direcció General de Recerca i Innovació del Govern Balear (AAEE039/2017).


### Notes

Any additional relevant notes should be placed here.


## ACKNOWLEDGMENTS

We thank the CTI (UIB) for computational facilities and allocation of computer time. We thank the Vice-Rector for Research and International Relations of the University of the Balearic Islands for the financial support in setting up the single-crystal X-ray diffraction facility.

## REFERENCES


(1) James, S.L.; Adams, C. J.; Bolm, C.; Braga, D.; Collier, P.; Friscic, F.; Grepioni, F.; Harris, K. D. M.; Hyett, G.; Jones, W.; Krebs, A.; Mack, J.; Maini, L.; Orpen, A. G.; Parkin, I. P.; Shearouse, W. C.; Steed, J. W.; Waddell, D. C. Mechanochemistry: opportunities for new and clearer synthesis. *Chem. Soc. Rev*. **2012**, *41*, 413 - 447.

(2) Delori, A.; Friscic, T.; Jones, W. The role of mechanochemistry and supramolecular design in the development of pharmaceutical materials. *Cryst. Eng. Comm.* **2012**, *14*, 2350-2362.

(3) Wang, M.; Tan, Q.; Li, J. Unveiling the role and mechanism of mechanochemical activation on lithium cobalt oxide powders from spent lithium-ion batteries. *Environ. Sci. Technol*., **2018**, *52*(22), 13136-13143.

(4) Danielis, M.; Colussi, S.; Leitenburg, C.; Soler, Ll.; Llorca, J.; Trovarelli, A. Outstanding methane oxidation performance of Pd-embeded ceria catalysts prepared by a one-step dry ball-milling method. *Angew. Chem. Int. Ed.* **2018**, *57*, 10212 –10216.

(5) Martínez, L.; Benito, M.; Mata, I.; Soler, Ll.; Molins, E.; Llorca, J. Preparation and photocatalytic activity of Au/$TiO_2$ lyogels for hydrogen production. *Sust. Energy Fuels* **2018**, *2*, 2284 – 2295.

(6) Li, P. Cheng, F-F, Xiong, W-W., Zhang, Q. New synthethic strategies to prepare metal-organic frameworks. *Inorg. Chem. Front*., **2018**, *5*, 2693–2708.

(7) Strukil, V.; Igrc, M. D.; Fábián, L. Eckert-Maksic, Childs, S. L.; Reid, D. G.; Duer, M. J.; Halasz, I.; Mottillo, C.; Friscic, T. A model for a solvent-free synthetic organic research labortory: click-mechanosynthesis and structural characterization of thioureas without bulk solvents. *Green Chem*., **2012**, *14*, 2462–2473.

(8) Braga, D.; Giaffreda, S. L.; Grepioni, F.; Pettersen, A.; Maini, L.; Curzi, M.; Polito, M. Mechanochemical preparation of molecular and supramolecular organometallic materials and coordination networks. *Dalton Trans.*, **2006**, 1249–1263.

(9) Jones, W.; Eddleston, M. D. Introductory Lecture: Mechanochemistry, a versatile synthesis strategy for new materials. *Faraday Discuss.*, **2014**, *170*, 9–34.

(10) Jayant Dengale, S.; Grohganz, H.; Rades, T.; Löbmann, K. Recent advances in co-amorphous drug formulations. *Adv. Drug Deliv. Rev*. **2016**, *100*, 116-125.

(11) Karagianni, A.; Kachrimanis, K.; Nikolakakis, I. Co-amorphous solid dispersions for solubility and absorption improvement of drugs: composition, preparation, characterization and formulations for oral delivery. *Pharmaceutics* **2018**, *10*, 98.

(12) Dai, X-L.; Chen, J-M.; Lu, Tong-Bu. Pharmaceutical cocrystallization: an effective approach to modulate the physicochemical properties of solid-state drugs. *CrystEngComm*, **2018**, *20*, 5292–5316.

(13) Hoogsteen, K. The structure of crystals containing a hydrogen-bonded complex of 1-methylthymine and 9-methyladenine. *Acta Cryst*. **1959**, *12*, 822.

(14) Katz, L.; Tomita, K-I.; Rich, R. The molecular structure of the crystalline complex ethyladenine: methyl-bromouracil. *J. Mol. Biol*. **1965**, *13*, 340 – 350.;

(15) Katz, L.; Tomita, K-I.; Rich, R. The crystal structure of the intermolecular complex 9-ethyladenine:1-Methyl-5-bromouracil. *Acta Cryst*. **1966**, *21*, 754.

(16) Tomita, K-I.; Katz, L.; Rich. R. Crystal structure of the intermolecular complex 9-ethyladenine:1-methyl-5-fluorouracil. *J. Mol. Biol.* **1967**, *30*, 545.

(17) Sakore, T. D.; Tavale, S. S.; Sobell, H. M. Base-pairing configurations betweens purines and pyrimidines in the solid state. *J. Mol. Biol*. **1969**, *43*, 361-374.;

(18) Shieh, H-S.; Voet, D. X-ray crystal structure of the molecular complex 9-Ethyladenine - parabanic acid-oxaluric acid monohydrate. *Acta Cryst*. **1975**, *B41*, 2192.

(19) Sagstuen, E.; Close, D.M. An ESR study of irradiated 1:1 cocrystal of 9-ethyladenine:5,5diethylbarbituric acid (barbital) at 295 K. *J. Chem. Phys*. **1983**, *79*, 117.

(20) Thompson, L. J.; Elias, N.; Male, L.; Tremayne, M. Supramolecular behavior of adenine with succinic, fumaric, and maleic acids: Tautomerism, cocrystallization, salt formation, and solvation. *Cryst. Growth. Des.* **2013**, *13*, 1464.

(21) Etter, M. C.; Reutzel, S. M.; Choo, C.G. Self-organization of adenine and thymine in the solid state. *J. Am. Chem. Soc.*, **1993**, *115* (10), 4411–4412.

(22) Koch, E. S.; McKenna, K. A.; Kim, H. J.; Young, V. G. Thymine cocrystals based on DNA-inspired binding motifs. *CrystEngComm*. **2017**, *19*, 5679-5685.
(23) McHugh, C.; Erxleben, A. Supramolecular structures and tautomerism of carboxylate salts of adenine and pharmaceutically relevant $N^6$-substituted adenine. *Cryst. Growth Des*. **2011**, *11*, 5096–5104.
(24) Izzatti Nadzri, N.; Hanim Sabri, N.; Lee, V. S.; Abdul Halim, S. N. 5-Fluorouracil co-crystals and their potential anti-cancer activities calculated by molecular docking studies. *J Chem. Crystallogr*. **2016**, *46*, 144–154.
(25) De Vries, E. J. C.; Kantengwa, S.; Ayamine, A.; Báthori, N. B. Testing the limits of synthon engineering: salts of salicylic acid and sulfosalicylic acid with nucleobases and derivatives. *CrystEngComm*, **2016**, *18*, 7573 – 7573.
(26) Pedireddi, V. R.; Ranganathan, A.; Ganesh. K. N. Cyanurate mimics of hydrogen-bonding patterns of nucleic bases: crystal structure of a 1:1 molecular complex of 9-ethyladenine and N-methylcyanuric acid. *Org. Lett*. **2001**, 3(1), 99-102.
(27) Sagstuen, E.; Close, D.M. An ESR study of irradiated 1:1 cocrystal of 9-ethyladenine:5,5diethylbarbituric acid (barbital) at 295 K. *J. Chem. Phys*. **1983**, *79*, 117.
(28) Kumar, J.; Awasthi, S.; Verma, S. Contrasting crystallographic signatures of 9-carboxypropyl adeninium cation: adenine dimerization vs carboxylic group interaction. *Cryst. Growth Des*., **2010**, *10*, 3555-3561.
(29) P. H. Stahl, P. H.; C. G. Wermuth, C. G. Ed., Handbook of Pharmaceutical Salts: Properties, Selection and Use, Weinheim/Zürich:Wiley-VCH/VHCA, 2002.
(30) García-Raso, A.; Fiol, J. J.; Bádenas, F.; Solans, X.; Font-Bardia, M. Reaction of trimethylene–bisadenine with $d^{10}$ divalent cations. *Polyhedron* **1999**, *18*, 765-772.
(31) Oxford Diffraction Ltd., CRYSALISPro Software System, 171.32 ed., Oxford, UK.
(32) SADABS, Bruker-AXS, Version 1, Bruker AXS Inc., Madison, WI, 2004.
(33) Coppens, P.; Leiserowitz, L.; Rabinovich, D. Calculation of absorption corrections for camera and diffractometer data. *Acta Crystallogr.* **1965**, *18* (6), 1035–1038.
(34) Walker, N.; Stuart, D. An empiricial method for correcting diffractometer data for absorption effects. *Acta Crystallogr.* **1983**, *A39* (1), 158–166.
(35) Farrugia, L. J. WinGX suite for small-molecule single-crystal crystallography. *J. Appl. Crystallogr.* **1999**, *32* (4), 837–838.
(36) Sheldrick, G. M. A short history of SHELX. *Acta Crystallogr.* **2008**, *A64* (1), 112–122.
(37) Altomare, A.; Burla, M. C.; Camalli, M.; Cascarano, G. L.; Giacovazzo, C.; Guagliardi, A.; Moliterni, A. G. G.; Polidori, G.; Spagna, R. SIR97: a new tool for crystal structure determination and refinament. *J. Appl. Crystallogr.* **1999**, *32* (1), 115–119.
(38) Sheldrick, G. M. Crystal structure refinament with SHELXL. *Acta Crystallogr.* **2015**, *C71* (1), 3–8.
(39) G. M. Sheldrick, SHELXL-2017/1, Program for the Solution of Crystal Structures, University of Göttingen, Germany, 2017.
(40) Spek, A. L. Single-crystal structure validation with the program PLATON. *J. Appl. Crystallogr.* **2003**, *36* (1), 7–13.
(41) Gaussian 09, Revision C.01, M. J. Frisch, G. W. Trucks, H. B. Schlegel, G. E. Scuseria, M. A. Robb, J. R. Cheeseman, G. Scalmani, V. Barone, B. Mennucci, G. A. Petersson, H. Nakatsuji, M. Caricato, X. Li, H. P. Hratchian, A. F. Izmaylov, J. Bloino, G. Zheng, J. L. Sonnenberg, M. Hada, M. Ehara, K. Toyota, R. Fukuda, J. Hasegawa, M. Ishida, T. Nakajima, Y. Honda, O. Kitao, H. Nakai, T. Vreven, J. A. Montgomery, Jr., J. E. Peralta, F. Ogliaro, M. Bearpark, J. J. Heyd, E. Brothers, K. N. Kudin, V. N. Staroverov, R. Kobayashi, J. Normand, K. Raghavachari, A. Rendell, J. C. Burant, S. S. Iyengar, J. Tomasi, M. Cossi, N. Rega, J. M. Millam, M. Klene, J. E. Knox, J. B. Cross, V. Bakken, C. Adamo, J. Jaramillo, R. Gomperts, R. E. Stratmann, O. Yazyev, A. J. Austin, R. Cammi, C. Pomelli, J. W. Ochterski, R. L. Martin, K. Morokuma, V. G. Zakrzewski, G. A. Voth, P. Salvador, J. J. Dannenberg, S. Dapprich, A. D. Daniels, Ö. Farkas, J. B. Foresman, J. V. Ortiz, J. Cioslowski, and D. J. Fox, Gaussian, Inc., Wallingford CT, 2009.
(42) Becke, A.D. A new mixing of Hartree-Fock and local density functional theories. *J. Chem. Phys*. **1993**, *98*, 5648-5652.
(43) Lee, C.; Yang, W.; Parr, R.G. Development of the Colle-Salvetti correlation-energy formula into a functional of the electron density. *Phys. Rev. B* **1988,** *37*, 785-789.

(44) Stephens, P.J.; Devlin, F.J.; Chabalowski, C.F.; Frisch, M.J. Ab initio calculation of vibrational absorption and circular dichroism spectra using density functional force fields. *J. Phys. Chem*. **1994**, *98*, 11623-11627.
(45) Mahmoudi, G.; Seth, S. K.; Bauza, A.; Zubkov, F. I.; Gurbanov, A. V.; White, J.; Stilinovic, V.; Doert T.; Frontera, A. Pb···X (X = N, S, I) tetrel bonding interactions in Pb(II) complexes: X-ray characterization, Hirshfeld surfaces and DFT calculations. *CrystEngComm*, **2018**, *20*, 2812-2821.
(46) Martínez-Benito, C.; Bauzá, A.; Lago, A. B.; Ruiz-Pérez, C.; Jiménez, C. A.; Torres, M. E.; Frontera, A.; Pasán, J. Anion−π Interactions in Hollow Crystals of a Copper(II)-Cyamelurate Coordination Complex. *Cryst. Growth Des*., **2018**, *18*, 2636-2644.
(47) Roy, S.; Drew, M. G. B.; Bauzá, A.; Frontera, A.; Chattopadhyay, S. Formation of a water-mediated assembly of two neutral copper(II) Schiff base fragments with a $Cu_2(NCS)_4$ moiety: exploration of non-covalent C-H···π(bimetallo ring) interactions. *CrystEngComm*, **2018**, *20*, 1679-1689.
(48) Ghosh, S.; Biswas, S.; Bauzá, A.; Barceló-Oliver, M.; Frontera, A.; Ghosh, A. Use of metalloligands [CuL] ($H_2L$ = salen type di-Schiff bases) in the formation of heterobimetallic copper(II)-uranyl complexes: Photo-physical investigations, structural variations and theorical calculations. *Inorg. Chem*., **2013**, *52*, 7508-7523.
(49) Boys, S. F.; Bernardi, F. The calculation of small molecular interactions by the differences of separate total energies. Some procedures with reduced errors. *Mol. Phys*., **1970**, *19*, 553-566.
(50) Keith, T. A. AIMAll (Version 13.05.06), TK Gristmill Software, Overland Park, KS, 2013.
(51) Amantia, D.; Price, C.; Shipman, M. A.; Elsegood, M. R.J.; Clegg, W.; Houlton, A. Minor groove site coordination of adenine by platinum group metal ions: effects on basicity, base pairing, and electronic structure. *Inorg. Chem*. **2003**, *42*, 3047-3056.
(52) Cruz-Cabeza, A.J. Acid-base crystalline complexes and the p$K_a$ rule. *CrystEngComm* **2012**, *14*, 6362-6365.
(53) Burkard, M. E.; Turner, D. H.; Tinoco, J. I. The RNA World. Appendix 1: Structures of base pairs involving at least two hydrogen bonds. 2nd Edition. *Cold Spring Harb. Monogr. Arch.* **1999**, *37*, 675–680.
(54) Qi, L.; Gundersen, L. L.; Chamgordani, E. J.; Gorbitz, C. H. Watson–Crick base pairing in 9-methyladenine and ethylene-9,9′-diadenine structures with close to 70% solvent content. *CrystEngComm* **2016**, *18* (34), 6352–6357.
(55) Guenifa, F.; Bendjeddou, L.; Cherouana, A.; Dahaoui, S.; Lecomte, C. Bis(adeninium) bis(hydrogensulfate) sulfate. *Acta Crystallogr.* **2012**, E*68* (12), 837–838.
(56) Bunick, G.; Voet, D. The structure of 9-[3-3-indolyl)-propyl]adenine. A model for protein/nucleic acid interactions. *Acta Crystallogr*. **1982**, *B38* (2), 575–580.
(57) Ikonen, S.; Valkonen, A.; Kolehmainen, E. X-ray structures of five variably tert-butoxycarbonyl-substituted adenines and their liquid and solid-state NMR investigations. *J. Mol. Struct*. **2009**, *930* (1–3), 147–156.
(58) Hockova, D.; Buděšinsky, M.; Marek, R.; Marek, J.; Holy, A. Regioselective preparation of $N^7$- and $N^9$-alkyl derivatives of $N^6$-[(Dimethylamino)methylene]adenine bearing an active methylene group and their further derivatization leading to α-branched acyclic nucleoside analogues. *European J. Org. Chem*. **1999**, *10*, 2675–2682.
(59) Sinha, I.; Hepp, A.; Kosters, J.; Muller, J. Metal complexes of 6-pyrazolylpurine derivatives as models for metal-mediated base pairs. *J. Inorg. Biochem*. **2015**, 6–11.
(60) Arpalahti, J.; Klika, K. D. Eur. Platinum-nitrogen bond rearrangements in isomeric cis-$Pt^{II}(NH_3)_2$-bis(9-methyladenine) complexes under alkaline conditions. *J. Inorg. Chem*. **2003**, *23*, 4195–4201.
(61) García-Raso, A.; Fiol, J. J.; Alberti, F. M.; Lagos, Y.; Torres, M.; Barceló-Oliver, M.; Prieto, M. J.; Moreno, V.; Mata, I.; Molins, E.; Estarellas, C., Frontera, A.; Quiñonero, D.; Deyà, P. M. New chloride(dimethyl sulfoxide)iridium(III) complexes with $N^6$-substituted adenines – kinetic N(7) versus thermodynaimic N(9) coordinated adenine isomers. *Eur. J. Inorg. Chem*. **2010**, *36*, 5617–5628.
(62) Ghosh, K.; Sen, T.; Frohlich, R. Adenine-based receptor for dicarboxylic acids. *Tetrahedron Lett*. **2007**, *48* (39), 7022–7026.

(63) Nair, V.; S. G. Richardson, S. G. Utility of purinyl radicals in the synthesis of base-modified nucleosides and alkylpurines: 6-amino group replacement by H, Cl, Br, and I. *J. Org. Chem*. **1980**, *45*, 3974-3981.
(64) Johnson, S. L.; Rumon, K. A. Infrared spectra of solid 1:1 pyridine-benzoic acid complexes; the nature of the hydrogen bond as a function of the acid-base levels in the complex. *J. Phys. Chem.* **1965**, *69* (1), 74–86.
(65) Aakeroy, C. B.; Debra J. Salmon; Smith, M. M.; Desper, J. Cyanophenyloximes: reliable and versatile tools for hydrogen-bond directed supramolecular synthesis of cocrystals. *Cryst. Growth Des.* **2006**, *6* (4), 1033–1042.
(66) Vener, M. V.; Egorova, A. N.; Churakov, A. V.; Tsirelson, V. G. Intermolecular hydrogen bond energies in crystals evaluated using electron density properties: DFT computations with periodic boundary conditions. *J. Comput. Chem*. **2012**, *33*, 2303–2309.
(67) Espinosa, E., Lecomte, C.; Molins, E. Experimental electron density overlapping in hydrogen bonds: topology vs. energetics. *Chem. Phys. Lett*. **1999**, *300*, 745-748.
(68) Espinosa, E.; Alkorta, I.; Elguero, J.; Molins, E. From weak to strong interactions: A comprehensive analysis of the topological and energetic properties of the electron density distribution involving X-H···F_Y systems. *J. Chem. Phys.* **2002**, *117*, 5529-5542.
(69) Weinhold, F.; Klein, R. A. Anti-electrostatic hydrogen bonds. *Angew. Chem. Int. Ed*. **2014**, *53*, 11214-11217.
(70) Alkorta, I.; Mata, I.; Molins, E.; Espinosa, E. Charged versus neutral hydrogen-bonded complexes: Is there a difference in the nature of the hydrogen bonds? *Chem. Eur. J.* **2016**, *22*, 9226-0234.
(71) Carvajal, M. A.; García-Yoldi, I.; Novoa, J. J. Solvent-Mediated Intermolecular Bonds: Cation–Cation and Anion–Anion Interactions in Solution Showing the Signature of Chemical Bonds. *J. Mol. Struct.: THEOCHEM* **2005**, *727*, 181– 189.
(72) Benyong Lou, B.; Guo, X.; Lin, Q. Crystal Structure of the Dihydrogen Phosphate Salt of Ozagrel (Ozagrel=(E)-3-[4-(1H-Imidiazol-1-ylmethyl)phenyl]-2-Propenic Acid). *J. Chem. Crystallogr.* **2009**, *39*, 469– 473;
(73) Vazdar, M.; Vymetal, J.; Heyda, J.; Vondrasek, J.; Jungwirth, P. Like-Charge Guanidinium Pairing from Molecular Dynamics and ab Initio Calculations. *J. Phys. Chem. A* **2011**, *115*, 11193–11201.
(74) Mata, I.; Alkorta, I.; Molins, E.; Espinosa, E. Electrostatics at the origin of the stability of phosphate-phosphate complexes locked by hydrogen bonds. *ChemPhysChem* **2012**, *13*, 1421-1424.
(75) Alkorta, I.; Mata, I.; Molins, E.; Espinosa, E. Energetic, topological and electric field analyses of cation-cation nucleic acid interactions in Watson-Crick disposition. *ChemPhysChem*, **2019**, *20*, 148-158.
(76) Mata, I.; Alkorta, I.; Molins, E.; Espinosa, E. Tracing environment effects that influence the stability of anion-anion complexes: The case of phosphate-phosphate interactions. *Chem. Phys. Lett*. **2013**, *555*, 106-109.

For Table of Contents Use Only

# 9-Ethyladenine: Mechanochemical Synthesis, Characterization and DFT Calculations of Novel Cocrystals and Salts

## *Graphical abstract*

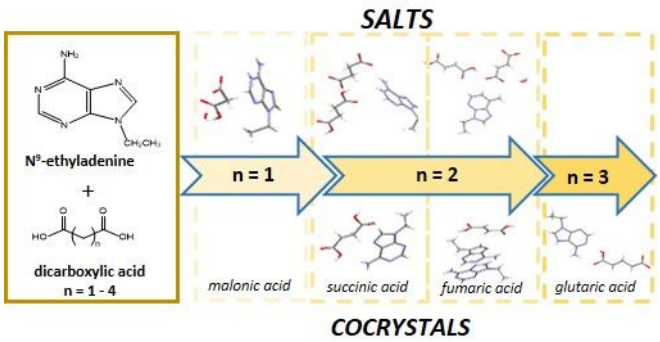


## *Synopsis*

Seven new cocrystals and salts of 9-ethyladenine with carboxylic acids of different alkylic chain length were synthesized. Their crystal structures, intermolecular interactions and thermal stability were analyzed together with the support of AIM and DFT calculations.